



VICTORIA UNIVERSITY
MELBOURNE AUSTRALIA

Nonstationary coherence characteristics of dual track road profile data

This is the Accepted version of the following publication

Lamb, Matthew and Rouillard, Vincent (2020) Nonstationary coherence characteristics of dual track road profile data. *Mechanical Systems and Signal Processing*, 140. ISSN 0888-3270

The publisher's official version can be found at
<https://www.sciencedirect.com/science/article/abs/pii/S0888327020301072>
Note that access to this version may require subscription.

Downloaded from VU Research Repository <https://vuir.vu.edu.au/40755/>

Nonstationary Coherence Characteristics of Dual Track Road Profile Data

M.J Lamb (PhD.)^{a*} and V. Rouillard^b (PhD.)

^{a,b} Mechanical Engineering, Victoria University, Footscray Park campus

PO Box 14428, MCMC 8001 Melbourne, Australia

^{a*}Corresponding Author Email: matthew.lamb@vu.edu.au

Abstract: The ability to accurately simulate the vibratory motion of transport vehicles is of great importance when designing vehicle components and product containment systems. Direct measurement and analysis of the vibrations is not always practical and laboratory testing using synthesized road elevation data is a common alternative, as is numerical simulation. However, no technique exists to generate realistic nonstationary dual track road elevation data.

This research focuses on uncovering statistical distributions that describe the nonstationary relationships between the left and right wheel-paths. Analysis of the short-time (nonstationary) coherence functions and instantaneous International Roughness Index (IRI) of measured road profile data provided distributions which describe variations in left to right wheel-path correlation and roughness variations for both tracks. The resulting distributions can be described with a three-parameter Weibull distribution and can be adopted to generate nonstationary dual wheel-path profile data that can be used to excite numerical vehicle models and physical vehicles via multi-axis simulators.

Keywords: coherence, nonstationary, road synthesis, multi-axial, vehicle simulation

1.0 Introduction

Numerically simulated and laboratory-based multi-axial testing and is becoming an increasingly important aspect of ground vehicle design and evaluation. It enables vehicles to be designed to withstand the rigors of travelling over uneven road surfaces and to achieve suitable ride conditions for the vehicle's occupants. The motion of the commercial vehicles also relates to the design of the consignments that they are transporting. To ensure that the products survive, protective packaging systems need to be tested to determine their ability to withstand the vibrations during of distribution and transport. This is especially the case for road transport which has been long-established as the primary source of damaging vibrations. It is also important to ensure that the protective packaging systems used do not place an unnecessary burden on the environment through the excessive use of materials. The ability to minimize packaging material use without increasing the risk of damage or failure of consignments requires an improved understanding of the distribution environment to support laboratory testing. This is a prime example of the importance of being able to accurately predict and simulate the multi-axial (heave, pitch and roll) vibratory motion of vehicles when travelling on particular road types or along particular routes [1, 2, 3]. Direct measurement and replication of heave, pitch and roll vibrations, although ideal are not always practical. Laboratory testing using synthesized road elevation data [4] is a common alternative as is numerical simulation. Numerical simulation in particular is becoming more attractive especially when it comes to studying the effects of various parameters such as vehicle geometry (wheel base, wheel track), vehicle and payload inertial characteristics (mass, center of gravity location, moments of inertia) and vehicle suspension properties. Numerical models describing the dynamic behavior of vehicles exist and can be adapted and developed to represent a variety of vehicle types. However, there is no suitable method for producing realistic dual track wheel-path excitation records that take into account not only the varying roughness of roads along particular routes [4], but also the relationship between the left and right wheel-paths which is primarily responsible for generating roll motion to the vehicle and its payload. Several authors have presented studies related to the synthesis of stationary dual wheel-path excitation records [5-8] with the vast majority using the coherence function between the left and right wheel-paths to synthesize partially

correlated dual path data. However, there is no consensus on a suitable coherence model and how the model may vary along the length of the road (nonstationarity).

The aim of this research is to uncover suitable statistical distributions which are capable of describing the nonstationary relationships between the left and right wheel-paths as well as the variations in their roughness. Such descriptors can then be adopted to generate realistic dual wheel-path profiles that can be used to excite both numerical vehicle models as well as physical vehicles via multi-axis road simulators.

The paper initially presents a brief review of various proposed coherence models that have been used to characterize the relationship between the left and right wheel-paths as a function of spatial frequency. The paper then addresses the need to develop a new approach that takes into account any variation in the left-right wheel-path coherence along the road. This requires the coherence to be described as a function of longitudinal distance as well as frequency. The paper also includes a study of the variations in roughness of both wheel-paths along the length of the road and any correlation roughness may have with variations in the left-right wheel-path coherence model.

2.0 Literature Review

It is now broadly accepted that the classic view of roads as an isotropic surface, first proposed by Dodds and Robson [9] then by Kamash and Robson [10], is not adequate [11]. Heath [12] uses the approximation of isotropy to express elevation cross-spectra as a function of the single-track elevation spectrum. Although useful at the time for providing an insight into the relationship between parallel tracks along a road, the isotropy assumption is conditional upon some admissibility tests. Further, comparison by Kamash and Robson [13] of their coherence model with some (limited) measured data contains significant disagreement with the isotropic model. Ammon [11] demonstrates the shortcomings of the isotropy assumption by comparing its coherence function with that computed from measured data (a single country road). Ammon [11] and Ammon and Bormann (cited in [14]), propose a more general surface model that is claimed to better match observations:

$$\gamma_{lr}^2(n, \rho) = \left[1 + \left(\frac{n\rho^a}{n_p} \right)^w \right]^{-2p} \quad (1)$$

Where n is the spatial frequency, ρ the track width, w the undulation exponent and n_p and p are arbitrary constants. Fitting of this model (1) to a number of measured data yielded a large scatter for the values of a , n_p and p [11]. Also, Ammon presents the coherence function over a narrow wavelength range of 10 m to 10 mm, which fails to take into account the longer important wavelengths which affect vehicle vibrations at higher speeds. Moreover, Ammon shows the coherence function to reach unity at a wavelength of 10 m which does not appear credible. The paper also fails to clearly explain how the random and bias errors associated with the computing of the coherence are addressed in his analysis of measured profile data. There is no mention of the length of the data analyzed nor the number of independent averages used to compute the coherence spectra.

For parallel tracks, coherence is described as the ratio the cross-spectra and the product of the auto spectra of the two wheel tracks. When the signal is random, as is the case for road profiles, there is a need to break the signal into sub-records to allow for spectral averaging which reduces errors contained within the instantaneous auto and cross spectra [15]. Invariably, the calculation of the coherence spectrum also involves both bias and random errors [15] that are a function of the number of averaged independent sub-records (segments or ensembles), N_d used to calculate the average cross and auto spectra as explained by Bendat and Piersol [15] and Carter et al. [16]. The bias error for the coherence spectrum, γ^2 , is given by:

$$b[\gamma_{lr}^2] \approx \frac{1}{N_d} (1 - \gamma_{lr}^2)^2 \quad (2)$$

and the normalized random error by (where s.d represents standard deviation):

$$\varepsilon[\gamma_{lr}^2] = \frac{s.d[\gamma_{lr}^2]}{\gamma_{lr}^2} \approx \frac{\sqrt{2}(1 - \gamma_{lr}^2)}{|\gamma_{lr}| \sqrt{N_d}} \quad (3)$$

These error functions are presented graphically in Figure 1 for various values of N_d .

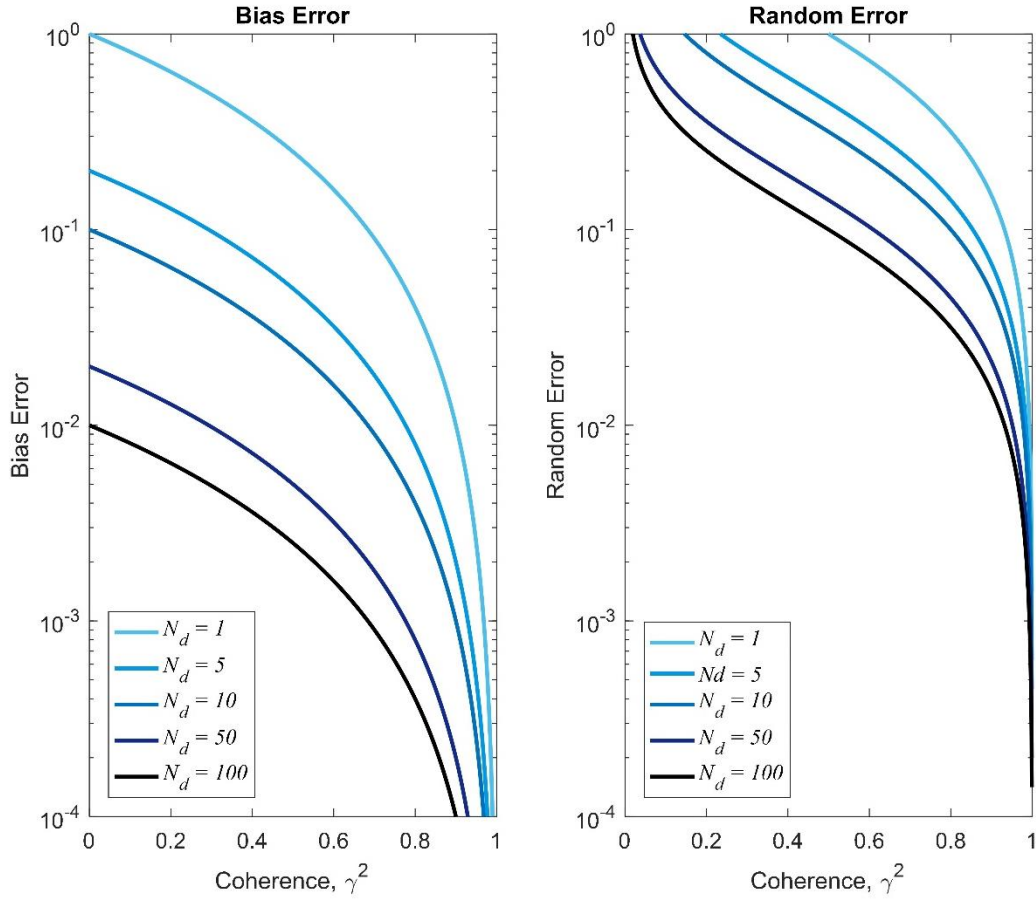


Figure 1. Left: Bias error of coherence; Right: Random error of coherence.

These errors are inextricably linked with the calculation of coherence spectral functions and must be addressed by carefully selecting the number of independent sub-records into which the signal is divided as well as the desired spatial frequency resolution, Δn , with which to compute the spectra according to:

$$\Delta n = \frac{1}{L_s} \quad (4)$$

Where L_s is the length of the independent sub-records. For records with a fixed overall length, this shows that a compromise must be reached to achieve both acceptable errors and sufficiently fine spectral resolution. This means that, if the signals (here left and right track profiles) are insufficiently long, coherence spectra with an acceptable frequency resolution cannot be obtained with any reasonable degree of accuracy. Consequently, validating coherence models on short road profile records is fraught with large statistical uncertainties.

Bogsjö [17] is the first to validate coherence models using acceptably large road profile records (between 5 and 45 km in length totaling 520 km) of varying quality (roughness). Bogsjö compares the coherence of measured profiles with the isotropic model which he found to be often inaccurate. A single-parameter model was proposed (5) and was found to accurately describe the coherence spectra of all 20 roads analyzed.

$$\gamma_{lr}^2(n, \rho) = e^{-2\rho b_l n} \quad (5)$$

Where n is the spatial frequency, ρ the track width and b_l an arbitrary constant. Bogsjö does mention independent (non-overlapped) sub-records and uses (2) to remove the bias error. The random error of the coherence function is not mentioned. A sub-record length of 32 m (giving a spatial frequency resolution of 0.031 m^{-1}) is used which, even for the shortest road, gives a reasonable number of independent averages ($N_d = 156$). Importantly, Bogsjö concludes that it is not possible to establish a relationship between the coherence spectrum and the road type (roughness). Despite the availability of long road segments, Bogsjö's work is limited to presenting the overall (average) coherence spectrum for each road and does not address the variation in coherence along the length of the road.

Můčka [14] presents a comprehensive overview of the evolution of the various coherence functions that aim at characterizing parallel wheel tracks. The author uses the 'unbiased squared-coherence' (note that coherence is properly defined by γ^2) of some 3,492 parallel track road records to evaluate the adequacy of various coherence functions (11 in all). He concludes that local road surface aberrations (bumps, potholes, etc.) do not affect the coherence spectra. This is unsurprising given that the coherence is based on spectral averages through which the occasional transients (aberrations) will be overwhelmed.

One important shortcoming of Můčka's analysis is the length of the road profile data he employs to validate the various coherence models. The sections are on average 145 m long which poses a serious limitation to the spectral resolution of the coherence and the errors associated with coherence calculations. Even by counting overlapped sub-records as independent, Můčka uses only seven overlapped sub-records leading to significant bias and random errors.

General observations from Múčka's evaluation of all 11 coherence models are summarized here.

- The model by Vlk (2000) (cited in Múčka [14]) is a single parameter model based on the isotropic assumption and as such is limited.
- The single-parameter exponential model identified by Bogsjö [17] was found to be well-suited to selected Swedish road sections by Bogsjö yet yielded large errors when compared by Múčka [14]. This may well be due to the short road elevation data sets used by Múčka as opposed to the 5 km + data sets used by Bogsjö [17].
- The two-parameter exponential model (Richter, 1990) (cited in Múčka [14]) is similar to the model introduced by Bogsjö [17] but includes a reference spatial frequency (that is not specified) as well as an arbitrary parameter while making no reference to wheel track.
- The three-parameter and two-parameter models proposed by Ammon [11] and Ammon and Bormann (1991) (cited in Múčka [14]) were found to yield the best results.
- Of the three models based on rational functions with one-, two- and three-parameters, introduced by Múčka [14], the single parameter function was said to best describe validation data set.

Despite the extensive work by Múčka [14], there is still no firm consensus on which coherence model is the most appropriate due to the limited data used for analysis. In saying this, Múčka's work is of value as it provides an extensive list of coherence models and indicates which are most likely to be suitable.

Overall, with the exception of Bogsjö [17], most of the published validation of the various proposed coherence models are carried-out on short or undeclared track profile lengths. This, as discussed, has a significant impact on the errors associated with the computed coherence spectra and introduces some substantial uncertainty when using them to validate coherence models. Bogsjö's results, although based on long track lengths (5 – 45 km), present overall (average) coherence spectra and do not address the nonstationarity of the spectra along the length of the road. The nonstationary nature of roads has been clearly established [18, 19, 20]; therefore, it is expected that any relationship between the left and right

wheel track will also be nonstationary. Understanding this nonstationary behavior is important when attempting to simulate realistic vehicle vibrations. This paper will seek to avoid the limitations of the previous studies by using a range of measured road profiles of adequate length to develop an accurate, yet practical, approach for describing coherence variations along parallel tracks.

3.0 Validation Data Set

The data used in this study includes 19 independent elevation data sets (totaling approximately 400 km) measured using an inertial profilometer along a wide variety of asphalted roads across the state of Victoria in Australia. Table 1 lists the details of each elevation record including an estimate of their average roughness which is described using the International Roughness Index (IRI) [21, 22, 23]. Each data set was measured across a track width of 1.5 m. The left wheel-path is the outer track and the right wheel-path is the inner track.

Table 1. Validation data set details.

Road Name	Road Type	Length [km]	IRI (left) [m/km]	IRI (right) [m/km]	IRI (mean) [m/km]
Princes Hwy East	Metro. Highway	20.3	1.5	1.4	1.5
Murray Valley Hwy	Country Highway	43.8	1.6	1.4	1.5
Princes Hwy East	Metro. Highway	22.9	1.7	1.7	1.7
Princes Hwy East	Metro. Highway	3.3	1.7	1.6	1.7
Murray Valley Hwy	Country Highway	47.7	1.9	1.7	1.8
Princes Hwy East	Metro. Highway	3.4	2.3	1.8	2.1
South Gippsland Hwy	Country Highway	11.3	2.3	2.0	2.2
South Gippsland Hwy	Country Highway	21.8	2.6	2.1	2.4
South Gippsland Hwy	Country Highway	15.0	3.1	2.6	2.9
Midland Hwy	Country Highway	14.0	3.3	3.2	3.3
South Gippsland Hwy	Country Highway	60.8	3.6	3.3	3.5
Daylesford - Malmsbury Rd	Country Road	25.4	4.0	3.3	3.7
Northern Hwy	Country Highway	5.0	4.1	3.8	4.0
Lismore - Skipton Rd	Country Road	32.6	4.2	3.7	4.0
Bendigo - Maryborough Rd	Country Road	22.3	4.3	3.8	4.1
Wiltshire Lane	Country Road	2.3	4.2	4.1	4.2
Pyrenees Hwy	Country Highway	12.4	4.8	4.2	4.5
Timboon - Port Campbell Road	Country Road	8.0	6.3	4.3	5.3
Euroa - Mansfield Rd	Country Road	8.3	6.1	5.0	5.6

The ability to establish the variation (nonstationarity) of the coherence function along the length of the road requires data sets of considerable length. Therefore, to enable such analysis, a number of records were concatenated to produce longer records. The roads were grouped with those of similar average roughness levels. When synthesizing road data in accordance with standards such as ISO8608, the main variable is average roughness level as the shape of the average power spectral density (PSD) function is fixed [24]. To allow for an investigation into any potential influence of road roughness on the left-right wheel-path coherence function four roads were created according to their nominal (IRI) roughness:

Road 1: Roads with a mean IRI of 2.1 or less

Road 2: Roads with a mean IRI of between 2.2 and 3.6

Road 3: Roads with a mean IRI of 3.7 or more

Road 4: Entire data set

The joining of the road elevation data also allowed for adequate analysis of rough roads which are inherently shorter.

Prior to concatenating the records, a high-pass filter (fourth order Butterworth set at $1/33 \text{ m}^{-1}$) was applied to each segment in order to ensure that the long wavelength errors, that are inherent to inertial profilometers [25], were removed from the data. In joining the segments, particular care was also taken to avoid the introduction of artefacts created by discontinuities at the extremities of each record. This was achieved by applying a short (32 point) windowing function (inverse Hanning) to each join in the record once concatenated. The PSD and coherence functions of each of the resulting records are presented in Figures 2 and 3. It is important to recall that these PSD and coherence functions do not reveal the variations that are caused by the nonstationary nature of the road profiles [26] but instead provide the average results for each road. It should also be noted that all results related to spatial frequencies below $1/33 \text{ m}^{-1}$ are deliberately excluded as the inertial profilometer used was not able to accurately capture this data; furthermore, the vibratory motion of the vehicle corresponding to elevation data at these spatial frequencies will be negligible.

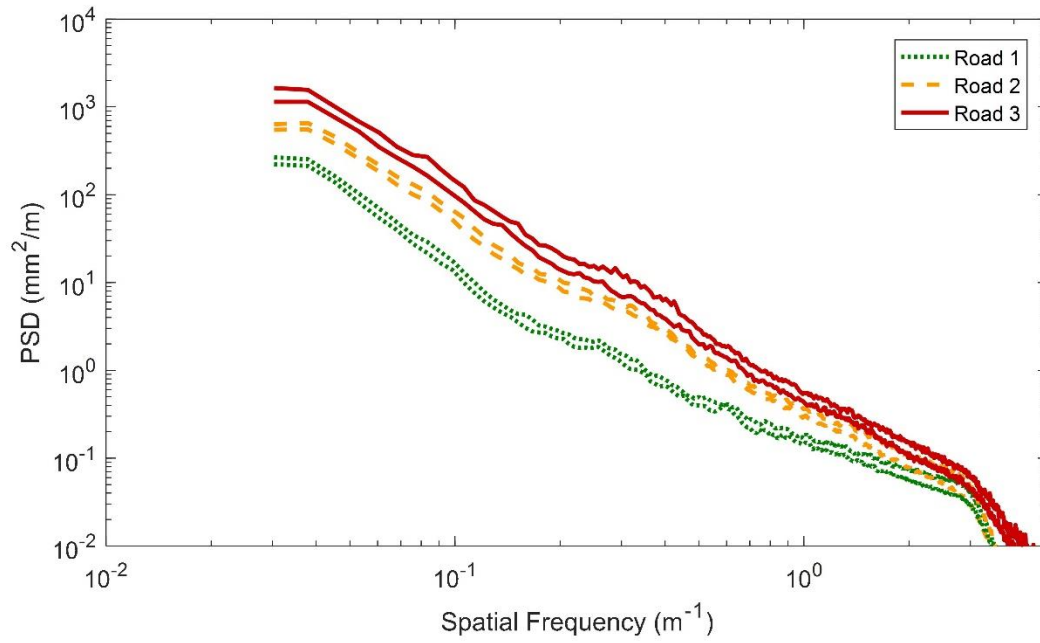


Figure 2. Average PSD function for each of the generated roads.

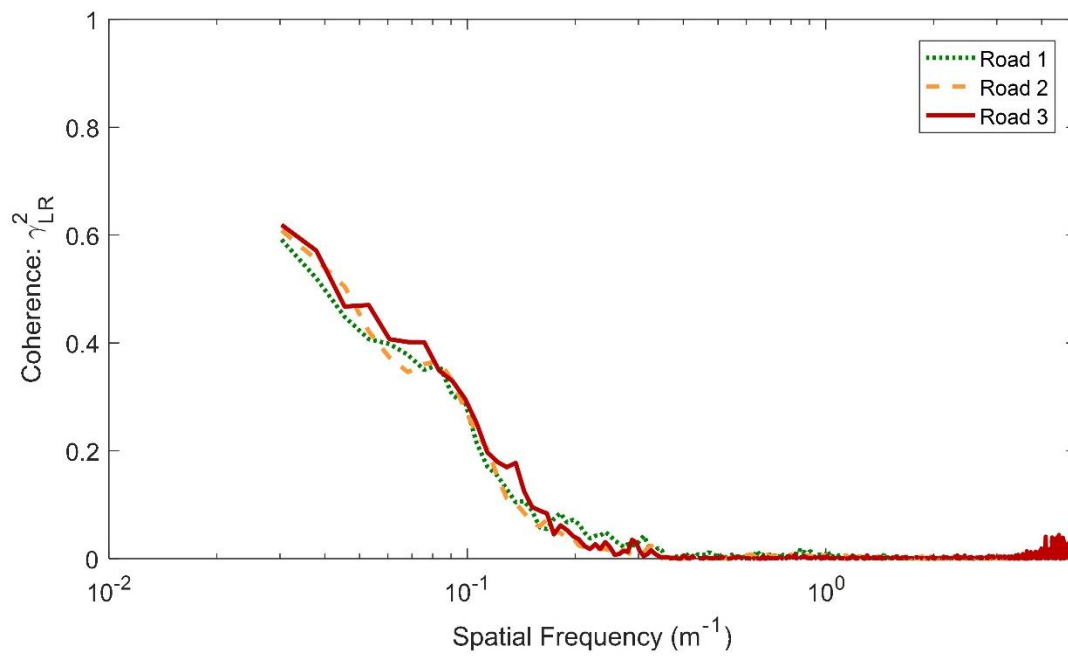


Figure 3. Average coherence functions for each of the generated roads.

4.0 Analyzing Coherence

There are two major parts to the analysis of the coherence function. The first is to establish the most appropriate coherence model for describing the measured left-right wheel-path coherence function. The second is to use this model to describe any variations in the coherence function along the length of the road. This requires a model which is easily defined and ideally includes as few arbitrary parameters as possible. Once a suitable model is found, variations in the coherence model will be compared with changes found in the IRI of the elevation data to establish whether or not the two are dependent.

4.1 Overall (average) coherence

To determine which models are likely best suited to the analysis, an average coherence function for each individual measurement record was found following a similar approach to that used by Múčka [14] but with records of greater segment length. This approach, despite not considering the potential nonstationary behavior of the coherence function, allows the models to be compared with the average coherence of each of the roads. In order to generate sufficient coherence estimates across the bandwidth of interest (i.e. to allow for accurate curve-fitting of coherence models) the spatial frequency resolution was set at 0.0075 m^{-1} (the reciprocal of four times the longest relevant wavelength in this instance) for all data sets. Furthermore, to contain the coherence uncertainty to acceptable levels, the number of independent sub-records, N_d , was set at 75 or greater. Consequently, the determination of the average coherence functions will be limited to the track elevations with a length of greater than 10 km ($75/0.0075 \text{ m}^{-1}$).

The analysis of suitable coherence models was achieved by comparing each against a cloud of coherence data. This cloud includes the left-right coherence functions of all individual road elevation records which are greater than 10 km in length. This will allow each coherence model to be compared as a fit of the average coherence function across the entire data set.

4.2 Nonstationary Coherence

Subsequent to the analysis of the average coherence function for each road, the four concatenated road records were subjected to short-length spatial frequency domain analysis to reveal the nonstationary

nature, if any, of the coherence function. The approach taken is to divide a road profile record into segments which themselves will be taken as quasi-stationary; hence representable by a single average (yet short-time) coherence function. This assumption was proven valid by Rouillard [19] who showed that nonstationary road data can be described by a number of independent quasi-stationary, Gaussian segments. Rouillard's work is supported by Bogsjo *et al.* [18] who suggest that shorter road segments are more likely to be homogeneous (stationary). Furthermore, Bogsjö *et al.* recognize that a compromise between the segment length and statistical uncertainties needs to be made when the data is non-homogeneous (nonstationary). This means that the segment lengths should be small enough to satisfy the stationarity assumption while being sufficiently long to produce coherence spectra with acceptably small errors (through spectral averaging). Further compromise is required to ensure that the spatial frequency resolution is also sufficiently small.

The analysis was implemented through the use of a modified version of the short-time Fourier transform which has the additional feature of averaging the individual spectra associated with each of the adjacent sub-records (L_s) to provide "short-time" (semi-instantaneous) coherence estimates for each segment. Figure 4 illustrates how the track profile data is separated into segments made-up of a series of sub-records on which Fourier analysis is performed to obtain the spectral estimates. Prior to performing any Fourier analysis, a Hanning window is applied to each sub-record to reduce side-lobe leakage [27]. To compensate for loss of information resulting from the application of the windowing function, overlapping of adjacent sub-records by a proportion (ol_{av}) is required [27, 28]. Typically at least 50% overlap is recommended when using the Hanning window [27]. In addition to averaging overlap (ol_{av}), the segments used for each short-time coherence function estimate can also be overlapped by a fraction, ol_{en} , to aid the visual interpretation of the results. When using the short-time Fourier transform, Randall [27] recommends using 75% overlap (ol_{en}).

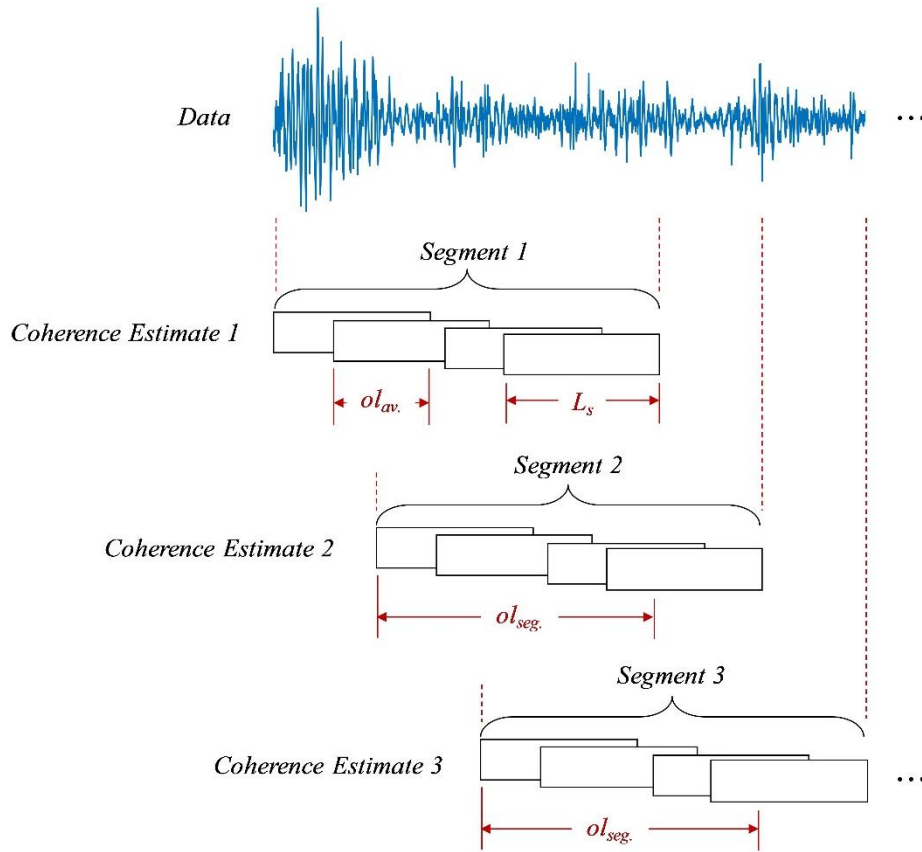


Figure 4. Schematic of nonstationary coherence tracking algorithm.

In this study, the averaging and ensemble overlaps were both set at 75% with 23 independent (90 overlapped) averages and the spatial frequency resolution was set at 0.0152 m^{-1} (the reciprocal of twice the longest relevant wavelength). These settings yield a spatial resolution of approximately 1,520 m. Although it is acknowledged that there may be some level of nonstationary behavior within the 1,520 m segments, these settings were found to provide the best compromise between spatial resolution and uncertainty in the estimated coherence functions. Since each coherence function estimate is obtained using a relatively high number of averages, no correction for bias had been applied to the data.

For more information on the modified short-time Fourier transform and its application when analyzing nonstationary random data, the reader is referred to Lamb [29].

5.0 Results

Of all the coherence function models presented in the literature, the single parameter model of Bogsjö [17] (5) showed the greatest potential as it has been successfully applied to large data sets and it allows the coherence function to be described by a single parameter. However, the work undertaken by Múčka [14] suggests that the three-parameter and two-parameter models proposed by Ammon [11] and Ammon and Bormann (cited in Múčka [14]), coherence models no. 5 (6) and 6 in Múčka (7), were better suited and that Múčka's own, no. 10, one parameter rational function model (8) adequately described the validation data set. The first stage of the research presented herein was to establish which of these models best describes that data set available and if the two and three parameter models provided a significantly improved description when compared to the single parameter models. This was achieved by estimating the average coherence function and fitting each of the coherence models to the resulting cloud. In effect, this is the same as fitting the model to the average coherence functions of the combined roads with the benefit of seeing the variation in coherence for each of the independent roads. The results from the analysis are presented in Figure 5 and include the other single-parameter model presented by Múčka, model no. 1 (9), for the purposes of completeness. The coherence function for the models shown in Figure 5 are listed in Table 2.

Table 2. Selected coherence models where b_i are arbitrary constants.

Model Name	Model Equation
Bogsjö [17]	$\gamma_{lr}^2(n, \rho) = e^{-2\rho b_1 n}$ (5)
Múčka [14] No. 5	$\gamma_{lr}^2(n, \rho) = \left[1 + (2\pi b_1 n)^{b_2}\right]^{b_3}$ (6)
Múčka [14] No. 6	$\gamma_{lr}^2(n, \rho) = \left[1 + 2\pi n^{b_1}\right]^{b_2}$ (7)
Múčka [14] No. 10	$\gamma_{lr}^2(n, \rho) = \frac{1}{(1 + 2\pi b_1 n)}$ (8)
Múčka [14] No. 1	$\gamma_{lr}^2(n, \rho) = \left(\frac{1}{1 + \left(\frac{2\pi\rho n}{b_1}\right)}\right)^2$ (9)

The results show that Bogsjö's [17] single parameter model is able to describe the coherence functions as well as the more complex two and three parameter models (Múčka [14] no. 5 and 6) of Ammon

(1992) and Ammon and Bormann (cited in Múčka [14]) and is far better suited than the other single parameter models presented in Múčka's review. A curve-fit of Bogsjö's model as extracted from the cloud data is compared to the average coherence function of Road 4 (concatenation of all road data in the validation data set) in Figure 6 to show that it is representative of the overall average coherence function.

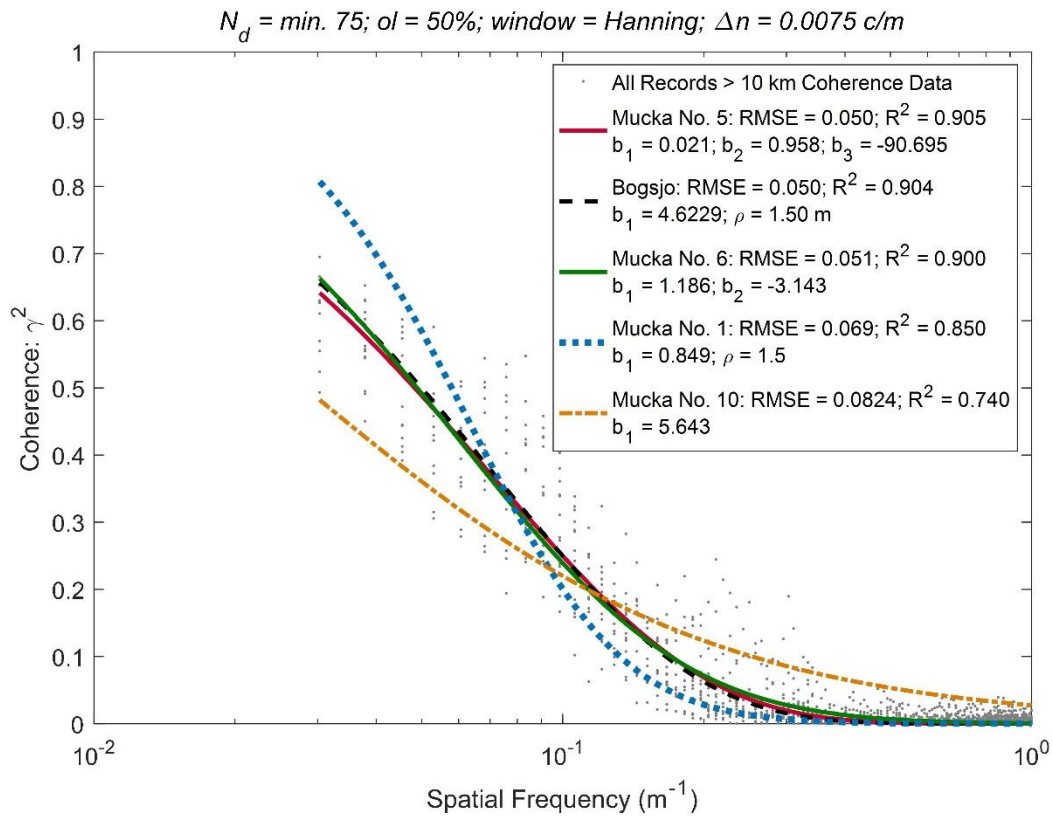


Figure 5. Suitability of various mathematical models for fitting average coherence function on cloud data.

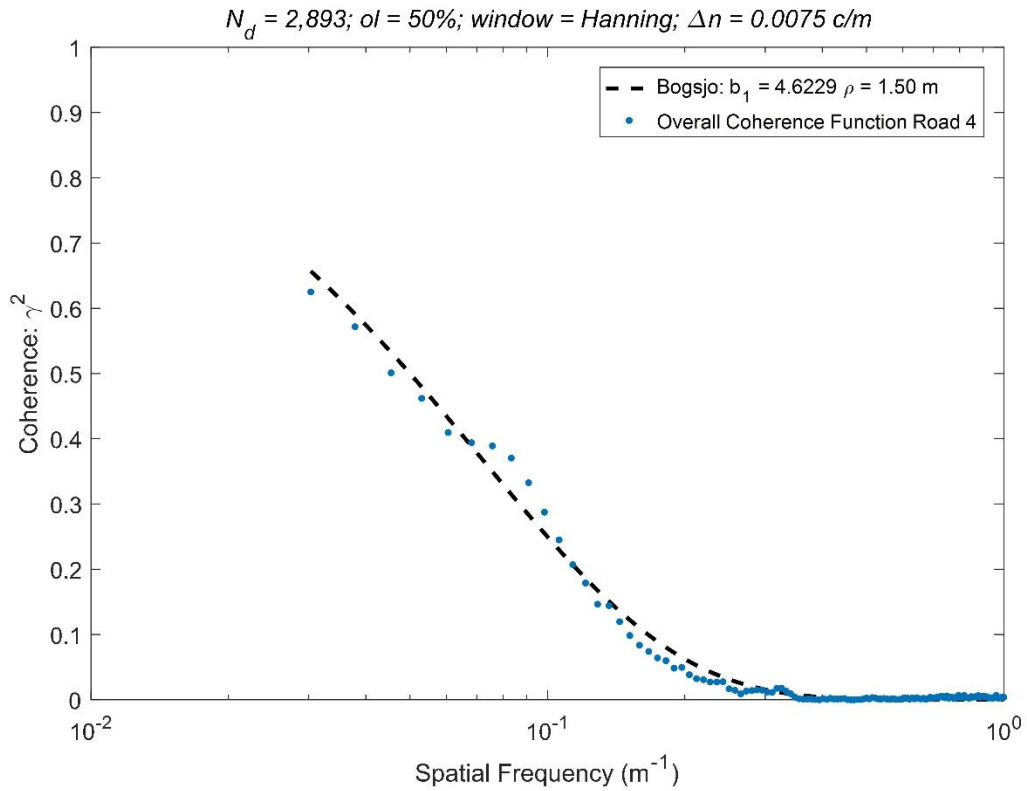


Figure 6. Comparison of single parameter function with average coherence function of Road 4 (entire data set).

Figure 7 compares the results obtained from the validation data set in this research to the results presented by Bogsjö [17]. As can be seen, despite the analysis being undertaken on two distinctly different data sets, there is strong agreement between the results in terms of both the average coherence function and the variation in the coherence functions across the roads analyzed.

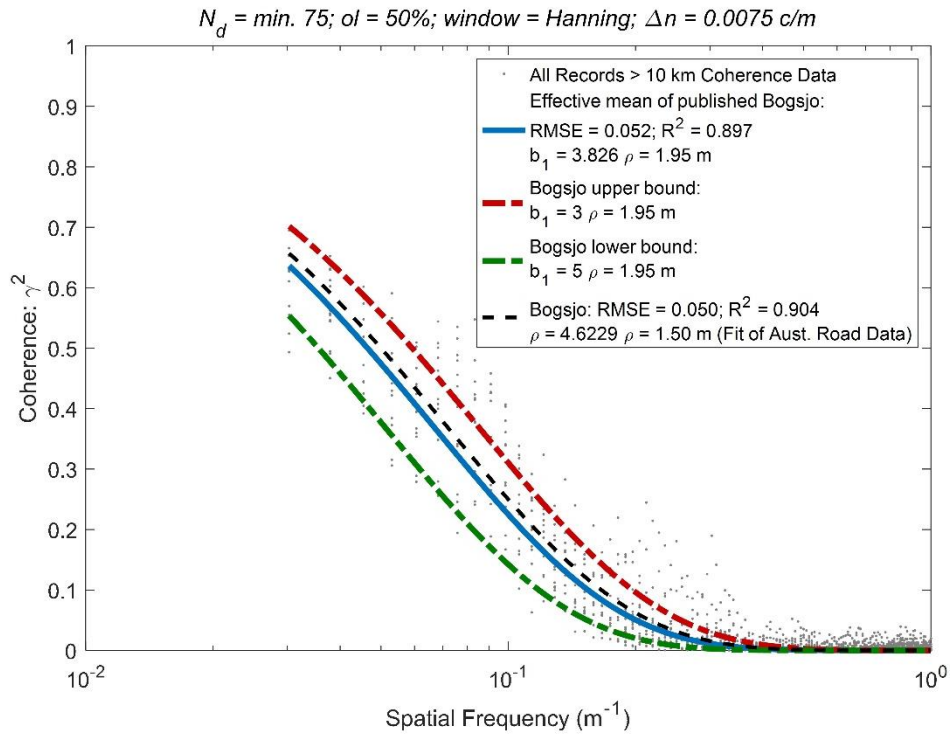


Figure 7. Comparison of findings from Australian road data with that of Bogsjö.

The next stage of the analysis was to attempt to characterize the variations (nonstationarity) in the coherence functions using the exponent b_1 of Bogsjö's [17] model as an index. Using the previously mentioned analysis parameters, coherence functions were estimated over approximately 380 m intervals, however, the true spatial resolution was only approximately 1,520 m (75% ensemble overlap). Figure 8 illustrates variations in the coherence function of Road 4 resulting from the nonstationary relationship between the left and right wheel-paths. Notice the significant variation in the coherence function which is not captured when assuming stationarity.

$N_d = 23$ (90 overlapped); $ol_{av} = 75\%$; STFT; $ol_{en} = 75\%$; window = Hanning; $\Delta n = 0.0152$ c/m

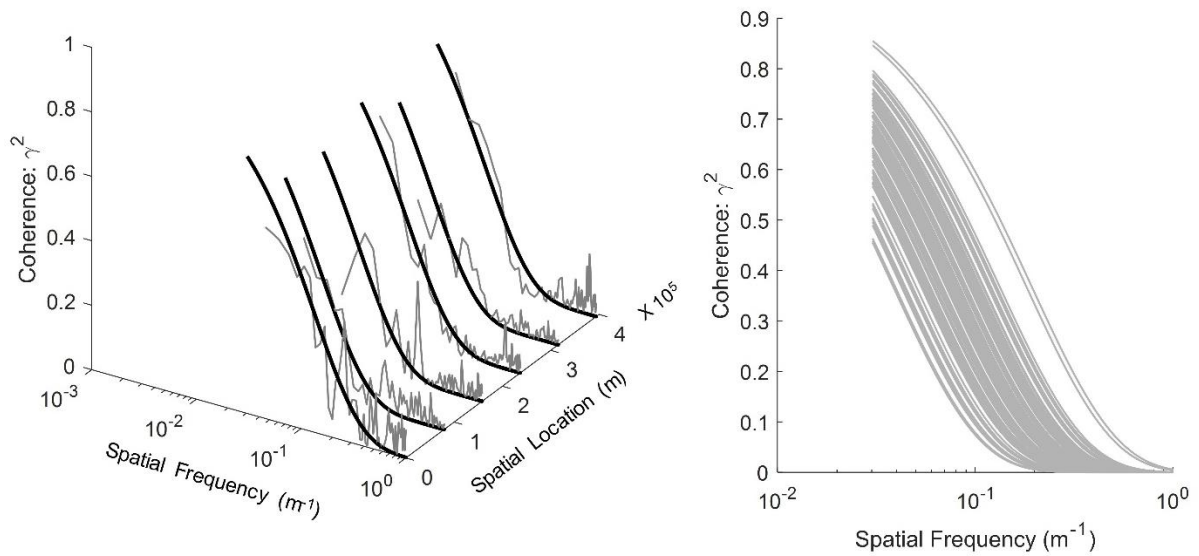


Figure 8. Nonstationary nature of the coherence function (left shows selected coherence functions and their curve-fits; right shows all coherence function curve-fits).

The distribution of the coherence function as described by Bogsjö's [17] model is presented in Figure 9 and is compared with the average IRI of the 1,520 m segments which the coherence was estimated from. Notice that the roads have been sorted from rough to smooth and that no correlation between roughness and the coherence function is evident. This lack of correlation is more clearly presented in Figure 10 which compares the exponent b_1 and the average of the left-right IRI directly.

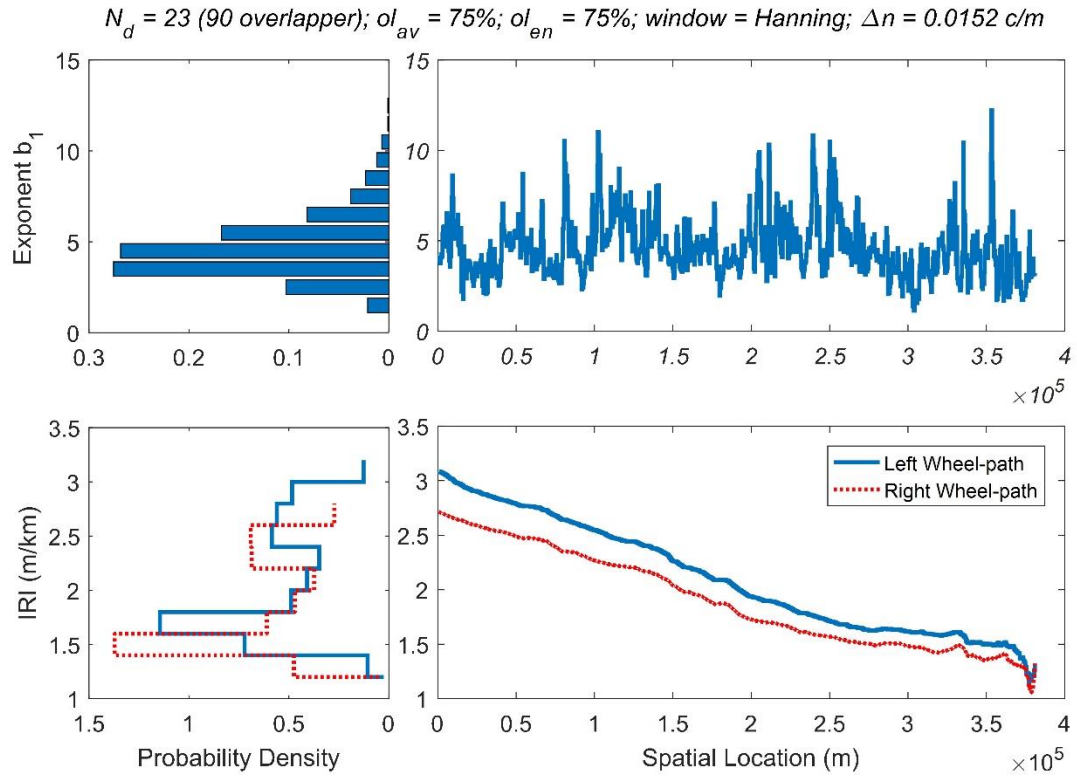


Figure 9. Top: Distribution of the coherence function using b_1 as the descriptor. Bottom: Distribution of average road roughness for analysis segments using IRI as a descriptor.

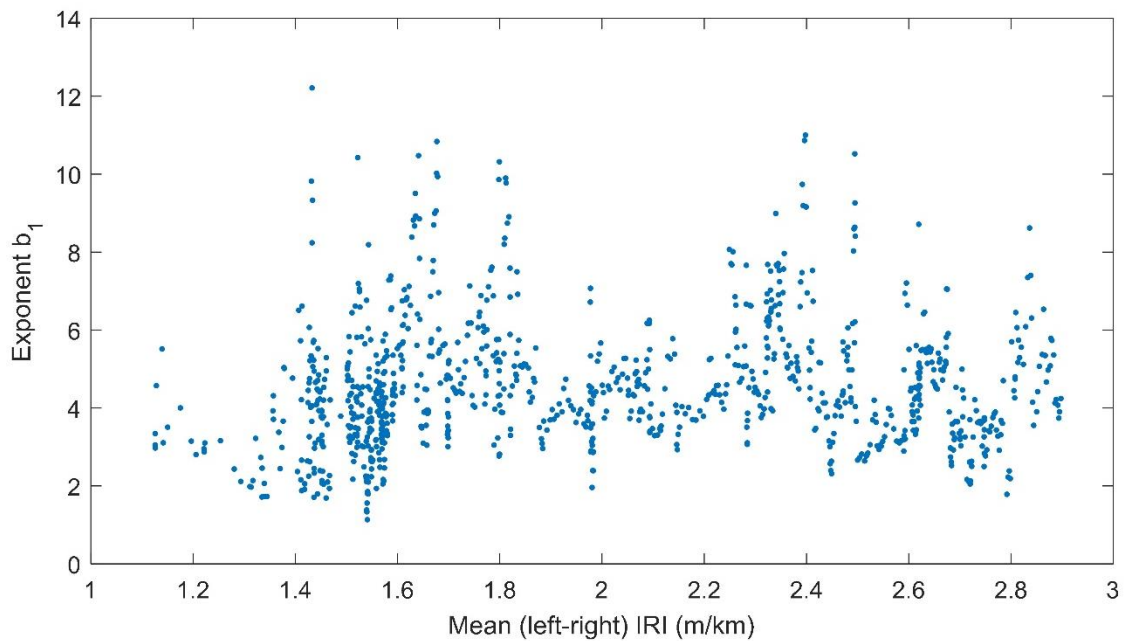


Figure 10. Correlation between b_1 and IRI.

In order to be able to synthesize dual wheel-path data for the purposes of multi-axial vibration simulation, a mathematical description of the distribution of the coherence function is required. There exists a number of mathematical distribution functions, two which have previously been shown to suitably describe a range of road vibration distributions are the modified Rayleigh [30] and the three-parameter Weibull [31]. With its ability to shift its shape, breadth (scale) and offset (location), the three parameter Weibull distribution is capable of fitting a wide range of data. Figure 11 presents the distribution of the coherence function for each of the roads in this study along with a mathematical model of the distribution of Road 4 (entire data set) achieved using a nonlinear least squares regression curve-fit of the three parameter Weibull distribution (10) [32].

$$f(x) = \frac{\beta}{\eta} \left(\frac{x - x_o}{\eta} \right)^{\beta-1} \cdot e^{-\left(\frac{x - x_o}{\eta} \right)^\beta} \quad (10)$$

Where β is the shape parameter, η is the scale parameter, x_o is the location parameter and x is the independent variable.

The resulting Weibull function enables suitable randomization of the coherence function when synthesizing nonstationary dual track road elevation data for road simulation purposes. In addition, Figure 11 again shows that, for the roads analyzed, the roughness of the road does not significantly influence the shape of the distribution of b_1 ; hence the shape and spread of the coherence function. This is significant as it allows the coherence function and road roughness level to be independently set when synthesizing the nonstationary dual track road records.

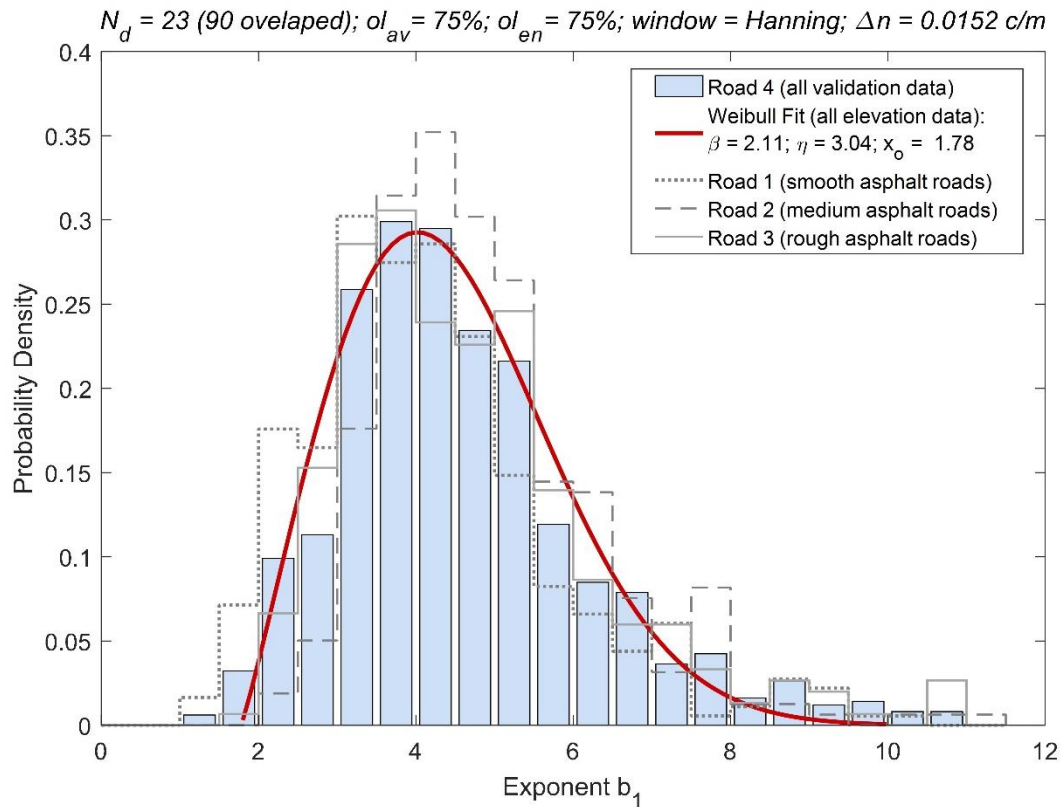


Figure 11. Probability density function (PDF) of the coherence function with for roads with varying levels of roughness

The only issue remaining to allow for the generation of synthesized nonstationary dual track data is the distribution of the road roughness for the left and right tracks. To achieve this, the instantaneous IRI values corresponding to each data point in roads 1-3 were determined and a 100 m moving average filter was applied. This resulted in average IRI estimates over 100 m intervals for each of the three roads. The resulting distributions from the analysis are presented in Figure 12 where they are compared to the closest fitting three-parameter Weibull distribution. These distributions allow asphalted roads of similar roughness levels (indicated by the average IRI) to the three test roads to be synthesized. With access to a greater number of road elevation records which cover a greater range of roughness levels, distributions which describe roads of any roughness could easily be achieved.

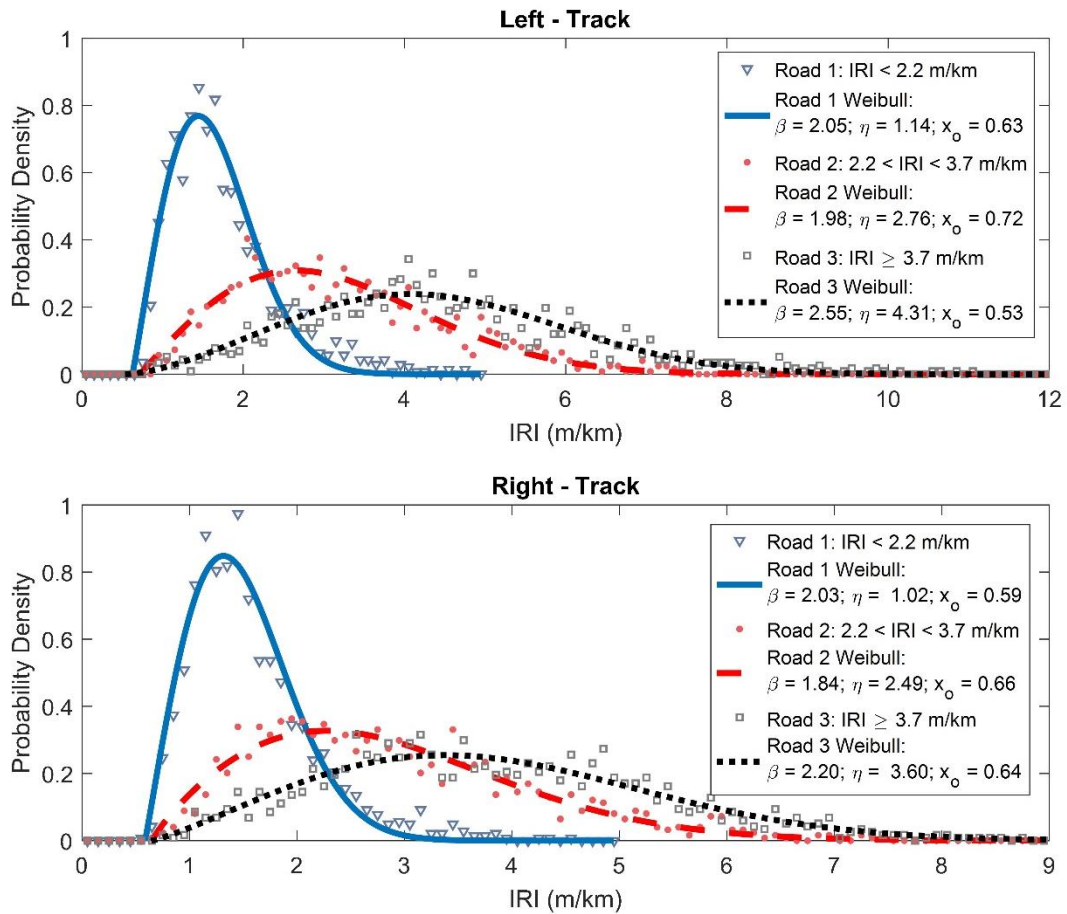


Figure 12. IRI distributions for roads with of various roughness content. Top: Left track. Bottom: Right track.

6.0 Conclusions

This research focused on uncovering statistical distributions that describe the nonstationary relationships between the left and right wheel-paths which will allow for the synthesis of realistic dual wheel-path profile data. The results showed that the coherence function which describes the correlation between the left and right wheel-path to be nonstationary and independent of road roughness. Simple three-parameter Weibull distribution models which describe the variation in the coherence function and the rough roughness (IRI) were established. These models make the synthesis of realistic dual track road elevation data possible for roads with average IRI values between 1.4 and 4 m/km. The synthesized models will be able to be used to excite numerical vehicle models and physical vehicles via multi-axis simulators for a range of applications including protective packaging design.

One limitation of the approach is that, as shown by the theoretical coherence error function, it is not possible to obtain accurate coherence spectra without compromise to the spatial frequency resolution and spatial resolution (short road segments). It may well be possible that a better description of the variations in left to right track relationship along the direction of travel can be achieved using spatial domain techniques which afford improved spatial resolution. Future work can address this by analysing the instantaneous camber of the road as the main descriptor of the correlation of the left and right wheel-paths. Further work should also focus on establishing a greater number of road roughness distributions to enable the synthesis of roads of elevated (IRI above 4m/km) roughness and for non-asphalt type roads.

References

1. Bernad, C., Laspalas, A., González, D., Núñez, J.L. and Buil, F. (2011). Transport vibration laboratory simulation: on the necessity of multiaxis testing. *Packaging Technology and Science*, 24(1), pp.1-14.
2. Batt, G. (2010). Use of simultaneous three axis vibration in simulation of the transport environment. *In International Transport Packaging Forum*.
3. Long, M.T., Rouillard, V., Lamb, M.J. and Sek, M.A. (2018). Characterising heave, pitch, and roll motion of road vehicles with principal component and frequency analysis. *Packaging Technology and Science*, 31(1), pp.3-13.
4. Rouillard, V., Sek, M.A. and Bruscella, B. (2001). Simulation of road surface profiles. *Journal of transportation engineering*, 127(3), pp.247-253.
5. Liu, X., Wang, H., Shan, Y. and He, T. (2015). Construction of road roughness in left and right wheel paths based on PSD and coherence function. *Mechanical Systems and Signal Processing*, 60, pp.668-677.
6. Bogsjö, K. (2007). Evaluation of stochastic models of parallel road tracks. *Probabilistic Engineering Mechanics*, 22(4), pp.362-370.

7. Yonglin, Z. and Jiafan, Z. (2006). Numerical simulation of stochastic road process using white noise filtration. *Mechanical Systems and Signal Processing*, 20(2), pp.363-372.
8. Feng, J., Zhang, X., Guo, K., Ma, F. and Karimi, H.R. (2013). A frequency compensation algorithm of four-wheel coherence random road. *Mathematical Problems in Engineering*.
9. Dodds, C.J. and Robson, J.D. (1973). The description of road surface roughness. *Journal of Sound and Vibration*, 31(2), pp.175-183.
10. Kamash, K.M.A. and Robson, J.D. (1977). Implications of isotropy in random surfaces. *Journal of Sound and Vibration*, 54(1), pp.131-145.
11. Ammon, D. (1992). Problems in road surface modelling. *Vehicle system dynamics*, 20(sup1), pp.28-41.
12. Heath, A.N. (1987). Application of the isotropic road roughness assumption. *Journal of Sound and Vibration*, 115(1), pp.131-144.
13. Kamash, K. and Robson, J.D. (1978). The application of isotropy in road surface modelling. *Journal of Sound and Vibration*, 57(1), pp.89-100.
14. Můčka, P. (2015). Model of coherence function of road unevenness in parallel tracks for vehicle simulation. *International Journal of Vehicle Design*, 67(1), pp.77-97.
15. Bendat, J.S., & Piersol, A.G. (1986). *Random data: analysis and measurement procedures*. 2nd Edition. John Wiley & Sons. New York
16. Carter, G., Knapp, C., & Nuttall, A. (1973). Estimation of the magnitude-squared coherence function via overlapped fast Fourier transform processing. *IEEE transactions on audio and electroacoustics*, 21(4), 337-344.
17. Bogsjö, K. (2008). Coherence of road roughness in left and right wheel-path. *Vehicle System Dynamics*, 46(S1), pp.599-609.
18. Bogsjö, K., Podgórski, K. and Rychlik, I. (2012). Models for road surface roughness. *Vehicle System Dynamics*, 50(5), pp.725-747.
19. Rouillard, V. (2008). Decomposing pavement profile data into a Gaussian Sequence. *Australian Road Research Board*.

20. Bruscella, B., Rouillard, V. and Sek, M. (1999). Analysis of road surface profiles. *Journal of Transportation Engineering*, 125(1), pp.55-59.
21. Sayers, M.W. (1995). On the calculation of international roughness index from longitudinal road profile. *Transportation Research Record*, (1501).
22. Sayers, M.W. and Karamihas, S.M. (1998). The little book of profiling: basic information about measuring and interpreting road profiles.
23. Johannesson, P. and Rychlik, I. (2012). *Modelling of road profiles using roughness indicators*.
24. Anon (2016). *International Standard 8608: Mechanical Vibration – Road Surface Profiles — Reporting of Measured Data*. International Organisation for Standardisation: Geneva.
25. Prem, H. (1988). A laser-based highway-speed road profile measuring system. *Vehicle System Dynamics*, 17(sup1), pp.300-304.
26. Rouillard, V. (2014). Quantifying the non-stationarity of vehicle vibrations with the run test. *Packaging Technology and Science*, 27(3), pp.203-219.
27. Randall, R.B. and Tech, B.A. (1987). *Frequency analysis*. Brüel & Kjær.
28. Bendat, J.S. & Piersol, A.G. (2000). *Random Data: Analysis and measurement procedures*. 3rd Edition. John Wiley & Sons. New York, p. 430.
29. Lamb, M. (2011). *Monitoring the structural integrity of packaging materials subjected to sustained random loads* (Doctoral dissertation, Victoria University).
30. Rouillard, V. and Sek, M.A. (2002). A statistical model for longitudinal road topography. *Road & Transport Research*, 11(3), p.17.
31. Garcia-Romeu-Martinez, M.A. and Rouillard, V. (2011). On the statistical distribution of road vehicle vibrations. *Packaging Technology and Science*, 24(8), pp.451-467.
32. Murthy, D.P., Xie, M. and Jiang, R. (2004). *Weibull models* (Vol. 505). John Wiley & Sons.